Cu(001) to HD energy transfer and translational to rotational energy conversion on surface scattering

L. V. Goncharova, J. Braun,[a] A. V. Ermakov, G. G. Bishop,[b] D.-M. Smilgies,[c] and B. J. Hinch
Department of Chemistry and Laboratory of Surface Modification, Rutgers University, Piscataway, New Jersey 08854

(Received 19 June 2001; accepted 24 July 2001)

Intense peaks are observed in angular intensity distributions for HD scattering from the Cu(001) surface. These can be ascribed to coherent diffraction with translational energy transfers of $\Delta E = 0, -11.0$, or 33.11 meV to molecular rotational energy. Time-of-flight spectra, at other scattering angles, display inelastic peaks that are assigned to phonon creation or annihilation processes with either the HD rotationally elastic or inelastic transitions. The HD phonon dispersion curves suggest a strong HD coupling both with surface Rayleigh modes and with bulk phonon modes of the metal surface. Comparisons of both elastic and inelastic scattering intensities are also made with those reported for the Ni(001) surface. To explain an apparent anomalous diffraction peak intensity ratio for Ni, a preferential coupling for the HD $J=0$ rotational state into a predissociation channel above the Ni surface is proposed. © *2001 American Institute of Physics.* [DOI: 10.1063/1.1403001]

I. INTRODUCTION

There have been many studies of hydrogen scattering from copper surfaces that look at various aspects of the molecule-surface interaction. State resolved dissociative adsorption[1,2] and thermal induced desorption studies[3–6] have looked at the dissociation/reassociation channel, whereas lower incident energy scattering has been used to investigate the influence of the physisorption potential well.[7–10] Fewer studies have been made of molecular diffraction and molecule-to-surface energy transfer for the copper substrates. The studies to be presented in this paper are all performed with incident translational energies (<100 meV) too low to promote dissociative adsorption. All work uses the ground vibrational state of hydrogen, and the incident molecular beam is rotationally cold, $J=0$. In addition, care was taken to avoid selective adsorption conditions; i.e., scattering conditions that can couple into bound state resonances through means of either rotation excitation or diffraction. In this incident energy regime energy redistribution and partial accommodation to the surface is observed. With the aid of a new apparatus we are able to resolve both separate and combined HD rotational excitation and surface phonon creation/annihilation events.

Combined hydrogen rotational excitation and inelastic phonon scattering was observed first for hydrogen scattering from the alkali halides. Allison and Feuerbacher performed time-of-flight measurements on scattering of H_2 and D_2 from a LiF (100) surface to find that single Rayleigh phonon scattering events can occur concurrently with molecular rotational transitions.[11] A similar result was seen for scattering of D_2 from NaF.[12] For HD–Ni (001) scattering,[13] perhaps surprisingly, little/few pure phonon scattering events were observed. In addition, the measured rotational and phonon loss features for HD on Ni(001)[13] give evidence for a coupling of the rotational transition to the transverse bulk edge phonons of the metal surface. Note also, unlike the symmetric (H_2, D_2) isomers, HD can undergo a facile $J=0$ to $J=1$ rotational excitation. We show that this is indeed a common occurrence on surface scattering. The rotationally inelastic ($J:0\rightarrow1$) ''specular'' peak can be of order 3–5 times larger than the elastic specular peak, just as was observed for the Cu(111),[7] Au(111),[7] Pt(111),[10,14] and Ag(111)[9,15] surfaces.

These studies concentrate on molecular HD scattering from a Cu(001) surface. The surface phonons of this substrate have been well characterized by inelastic He scattering studies.[16,17] This paper will focus on two main issues, namely the observed ratio of rotationally inelastic-to-elastic diffraction features, and the apparent dispersion of phonon modes observed with inelastic HD scattering. In both cases we shall make close comparison with the prior results for HD scattering from a Ni(001) surface.[13] The paper begins with a description of the new molecular beam scattering apparatus and other experimental details. The measured angular distributions for HD are presented and an ''inelastic Ewald'' construction is shown which aids in the assignment of the observed diffraction peaks. An asymmetry in diffraction peak intensities is discussed. HD-surface elastic and inelastic Debye–Waller factors are investigated. Time-of-flight resolved phonon dispersion curves along two high symmetry azimuths, measured with HD, are compared to those measured with He on the same Cu(001) surface. Finally we compare the results presented here with the data taken from the Ni surface.

II. EXPERIMENT

The apparatus for these experiments was primarily designed for studies of surfaces using both elastic diffraction

[a]Present address: Infineon Technologies, Balanstrasse 73, D-81541 Munich.
[b]Electronic mail: bishopgg@aol.com
[c]Present address: CHESS G-line, Cornell University, Ithaca, NY 14853.

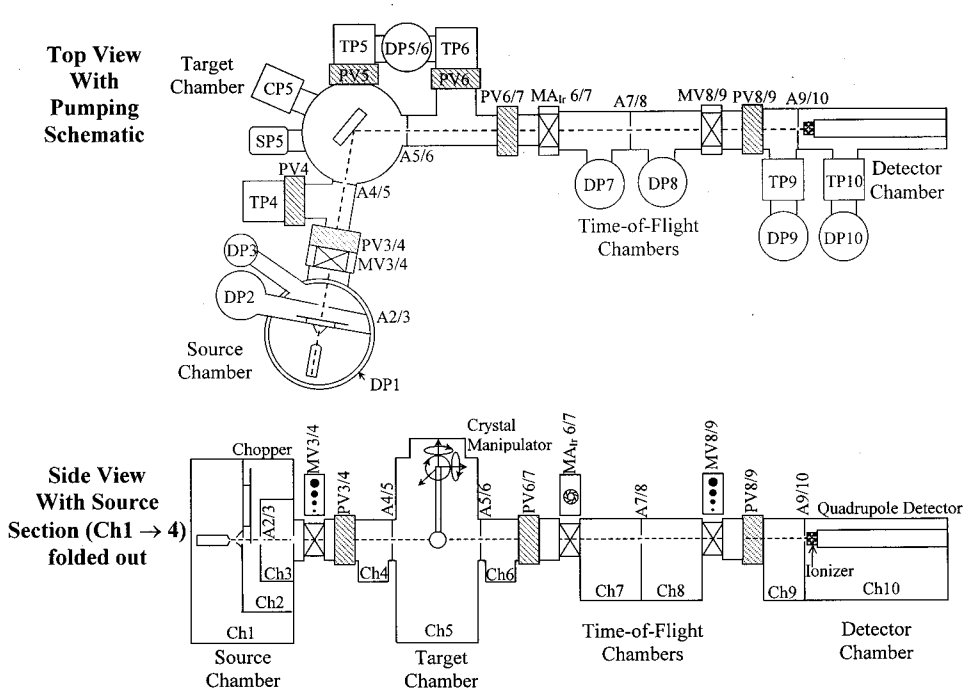

FIG. 1. Schematic of the beam scattering instrument in two different perspectives. The label numbers refer to the vacuum chamber numbers 1→10. The label letters refer to: DP–diffusion pump; A–aperture; MV (variable aperture) manual valve, PV–(electro-) pneumatic valve; TP–turbo molecular pump; SP-Ti sublimation pump; CP–cryopump; MA_{Ir}–manually controlled variable aperture (iris). A more detailed description of the components can be found in Table I.

and inelastic scattering of He atoms. In the majority of experiments described here an HD beam seeded in He is utilized. Specific details of this beam are discussed further below. The main components of the apparatus are a beam source chamber, an ultrahigh-vacuum chamber, a time-of-flight section, and a mass-resolved atom/molecule detector (see Fig. 1). More details of the specific components involved are presented in Table I.

First we describe typical experimental conditions for work with a supersonic helium beam (some helium scattering data are also presented in this work.) Ultrahigh purity He under high pressure (typically between 3 and 70 bar) is expanded into vacuum through an electron beam etched, 20 μm diameter, Pt nozzle. The energy of the surface incident helium atoms in the beam can be changed by varying the temperature of the nozzle, ($E_i = 5/2\, kT_{noz}$). T_{noz} can be controlled in the range of 40–330 K ($E_i = 10$–70 meV). Intrinsic to the supersonic expansion source, a skimmer is placed at a variable distance before the beam nozzle to separate the central section of the beam from the stray background gas pressure, and forming the boundary between a heavily pumped first chamber and a second chamber. The molecular beam passes through two further differentially pumped stages and is collimated again by the series of apertures (indicated as A2/3, MV3/4, and A4/5 in Fig. 1). Finally, when the beam enters the scattering chamber its size is usually determined by the diameter of aperture MV3/4. For the majority of data reported here, a 3.5 mm diameter aperture is utilized giving an angular spread of 0.11 °. Both smaller (less divergent) and broader (total surface illuminating) beams are also possible.

The UHV scattering chamber has a base pressure of order 1×10^{-10} mbar. The molecular beam impinges directly on a well-prepared crystalline surface and a small fraction of the back-scattered molecules (atoms) pass through another four stages of differential pumping (the time-of-flight section) to the detector chamber. The nominal angle subtended by the detector at the target is 0.12°. In this last chamber the scattered beam flux is measured using electron beam ionization (ionization region ~8 mm diameter), mass selection through an rf quadrupole mass spectrometer, and pulse counting after a channeltron multiplier. While a maximum specular intensity is not measured directly, as the detector saturates, the specular He count rate is in excess of 10 MHz from a clean Cu(001) surface with total reflectivity ~20% at $T_x \approx 130$ K. The base pressure in the detector chamber (#10) is of order 8×10^{-11} mbar. A considerable fraction of that is hydrogen (H_2). A high mass resolution (~1000) ensures no discernable count rate from mass 2 (H_2). Only a dark count rate (~5 cps) is observed around mass 4 (He), derived presumably from x-ray induced ionization.

For measurements of inelastic scattering rates a pulsed beam is used. A mechanical chopper in chamber (#2) can be lowered into the beam. A four-slit aluminum alloy disk, 203 mm in diameter, with gating fractions between 0.7% and 2.7% is used. The chopper disk rotation is driven by a water-cooled brushless dc motor, which is held in vacuum, and its rotation frequency can be varied easily in a range of 100–200 Hz without compromising the motor bearing lifetime. The gating fraction and rotation speed parameters allow independent variation of intensities and durations (widths) of the beam pulses. Beam pulse durations range from 9.5 μs (0.7%, 200 Hz) to 64.3 μs (2.7%, 100 Hz). A fast LED/

TABLE I. Apparatus components.

Component	Description	
	Backing pumps	
Pumps	Intermediate	Roughing
DP1 (Varian HS-20, 17 500 l/s, 22 000 l of He/s)	roots pump (Leybold RUVAC WSU-501, 350 CFM)	RP1 Alcatel 2063, 40 CFM
DP2 (Varian VHS-6, 2400 l/s)	-	RP2/3 Alcatel 2033,
DP3 (Alcatel Crystal 63, 200 l/s)	-	21 CFM
TP4 (Pfeiffer TMU260, 210 l/s)	DP4 (Edwards Diffstak 63/150	RP4/5/6 Alcatel 2033,
TP5 (Leybold TMP1000, 1000 l/s)	170 l/s)	21 CFM
TP6 (Pfeiffer TPU060, 56 l/s)	-	
SP5 (Ti sublimation pump)	-	-
CP5 (Varian, 4000 l/s cryopump)	-	-
DP7 (Varian VHS-4, 1200 l/s)	-	RP7/8 Alcatel 2033,
DP8 (Varian VHS-4, 1200 l/s)	-	21 CFM
TP9 (Pfeiffer TPU060, 56 l/s)	DP (Edwards Diffstak 63/150 170 l/s)	RP9 Alcatel 2008, 6 CFM
TP10 (Leybold TMP360, 340 l/s)	DP10 (Edwards Diffstak 63/150 170 l/s)	RP10 Alcatel 2012, 9 CFM
PV4, PV5, PV6	Electro-pneumatic security valves	
In-line Valves		
PV3/4, PV6/7, PV8/9	Electro-pneumatic valves (MDC GV1000)	
MV3/4, MV8/9	Variable aperture manual valves (0; 1; 3.5; 10 mm)	
In-line Apertures		
A2/3, A4/5, A5/6	Replaceable apertures, currently with 2.5; 8; 8 mm diam s	
A7/8, A9/10	Permanent apertures with 8; 8 mm diam s	
$MA_{Ir}6/7$	Iris (aperture variation in 0...13.5 mm range)	
Nozzle	Supersonic nozzle 20 μm diam, platinum	
Skimmer	0.5 mm diam, Ni (Beam Dynamics)	
Manipulator	6 axis manipulator based on Thermionics Northwest GP17 goniometer head with virtual tilt axis	
Detector	Extranuclear Quadrupole mass spectrometer, 0.75 in. diam. rf rods, axial ionization region and off-axial channeltron multiplier	

photodiode pair monitors the passing chopper disk slits and is used to initiate an electrical trigger pulse. This pulse initiates a programed delay time in the multichannel scalar (MCS). The time of arrival, or time-of-flight (TOF), of individual scattered and detected particles is then recorded during repeated cycling and/or beam pulses. Compensation for a small chopper-frequency-dependent time offset, caused by misalignment of the phototransistor position with the chopper slit center and beam position, is included with one fixed parameter in the data evaluation software. This parameter was established by the measurement of elastic scattering in TOF spectra at the surface specular reflection angle, for different chopper rotation frequencies. To achieve adequate signal-to-noise ratios in the TOF spectra, scattering measurement times have ranged between 3 and 180 min, depending on total beam fluxes and back-scattered fractions. Typical experimentally determined He-beam velocity resolutions, at example operation conditions, are presented in Table II.

TABLE II. Operating parameters and velocity resolutions of helium beams.

Nozzle temperature, K	He beam energy, meV	Nozzle pressure, bar	Chopper pulse frequencies, Hz	$\Delta v/v$, Velocity resolution, %
42	10	3	400	0.8
73	15	6	600	0.7
133	29	30	600	0.9
273	60	55	600	1.5

The sample is mounted on a commercial six-axis goniometer. Back-scattered intensity distributions can be measured as a function of the polar angles Θ, the tilt angle χ, or the azimuth Φ. Most routine total intensity distributions of the scattered He atoms are recorded with rotation of the crystal about an axis perpendicular to the plane containing both the incoming beam and detector (scattering plane). Angular distributions are thereby recorded as a function of the polar or incident angle, Θ_i, measured with respect to the surface normal (see Fig. 2). Typical measurement times for total intensity (nonenergy resolved) angular distributions are in the range of 3–8 min. ''Out-of-plane'' angular distributions can be recorded as a function of the polar angle Θ_i with the addition of a surface normal tilt out of the scattering plane. Repeated ''out-of-plane'' scans can also be used to raster across many scattering directions, thereby producing 2D scattered intensity images.

In addition to the total intensity angular distribution

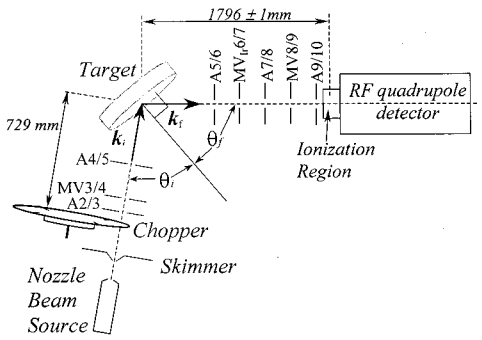

FIG. 2. Schematic view of the instrument scattering geometry with respect to the target. Only beam/resolution defining apertures are included. (Note: components are not to scale.)

scans described above, time-of-flight energy resolved polar angle scans are also readily achieved. This type of scan can be used to select for definite inelastic features. Such energy resolved scans are presented in Sec. III below.

For the measurements reported here, the Cu(001) sample was cleaned by cycles of ion bombardment at room temperature (30 min, Ne^+, 600 eV, 5 μA/cm^2) and annealing up to 675 K for 10 min followed by a final heating to 900 K. Sample heating is achieved through either radiative or electron beam heating from an adjacent tungsten filament. Sample cooling uses a liquid nitrogen reservoir and a flexible copper braid. Crystal temperatures, between 100 K and 900 K, are measured with a spot-welded Chromel-Alumel thermocouple tied to the crystal under tantalum supports. After cleaning, *in situ* Auger analysis, with a double pass cylindrical mirror analyzer, showed no measurable carbon, sulfur, or oxygen contaminants ($<$0.005 ML). Angular distributions recorded from the clean surface reveal specular diffraction peaks with full-width at half-maxima (FWHM) as small as 0.35°.

The high quality, low velocity spread, typical of the supersonic helium expansion, with $\Delta v/v \sim 1\%$, is carried over to the HD molecular beams by use of HD seeded in He. The molecular HD beam originates from a gas cylinder mixture of 5%H_2, 5%D_2, and 90% He. The gas mixture (at ~20–50 bar) is passed over a Mg granule catalyst which is heated to 600 K, thereby producing molecular HD. The time-of-flight energy analysis technique typically shows a $\Delta v/v$ for He and D_2 (mass 4) of order 1%. No attempt was made to evaluate the H_2 characteristics in the beam as the signal to noise ratio was anticipated to be poor. There is, however, no background interference to the signal at mass 3. HD is resolved clearly with $\Delta v/v$ typically ~1.5%.

The seeded beam, of HD (H_2 and D_2) in He, produces all HD molecules in the $J=0$ rotational state due to rotational relaxation in the expanding beam.[18] Rotational excitation of the molecules can occur only on scattering at the surface. Excitation from the $J=0$ to $J=1$ state ($J:0\rightarrow1$) is associated with a transfer of 11.063 meV of energy into the rotational degree of freedom. As the largest fraction of the molecular-Cu scattering is elastic (with respect to the surface-molecule energy transfers), the most intense features in our angular diffraction scans correspond to a $J:0\rightarrow1$ excitation, with zero parallel momentum exchange. The rotationally inelastic coherent scattering is detected at incident angles less than that of the truly elastic (specular) diffraction peak. These types of characteristic angular intensity distribution combined with the TOF have been used for calibration purposes. This calibration was achieved through TOF measurements of the rotationally elastically and inelastically (with rotational excitation) scattered molecules. The Appendix details the calibration procedure for determination of apparatus parameters. We concluded that the angle between incoming and outgoing beams is 99.0° ± 0.1° and the distances, crystal-detector, and chopper-detector, are 1.796 ± 0.001 m and 2.525 ± 0.001 m, respectively.

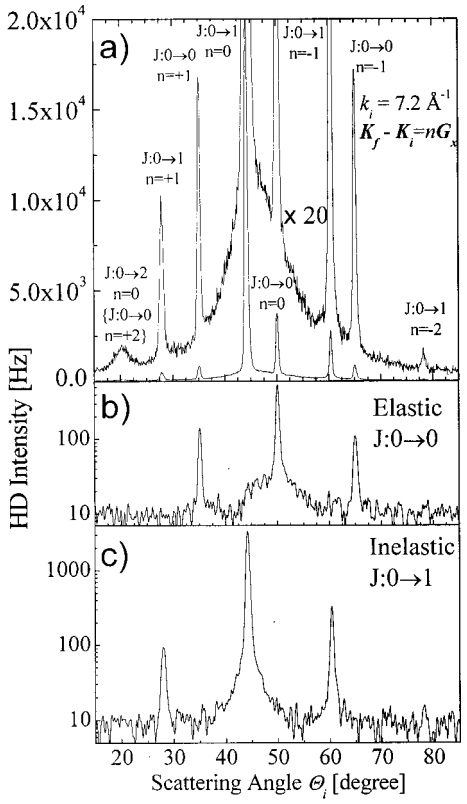

FIG. 3. Angular distributions for HD scattering in the $[1\bar{1}0]$ direction from the Cu(001) surface at $T_x = 323$ K, and $E_i = 36$ meV, $k_i = 7.2$ Å^{-1}. (a) The total intensity distribution shows many peaks, each is labeled with a rotational transition and a diffraction index. The lower panels show angular distributions with TOF energy selection. In (b) elastic ($\Delta J = 0$) and in (c) inelastic ($\Delta J = 1$) scattering channels are shown.

III. RESULTS

Figure 3(a) shows an observed angular distribution of the HD scattering intensity along the $[1\bar{1}0]$ azimuth. Each of the observed intensity peaks have been labeled with both a rotational transition (if any) and an in-plane diffraction order, *n*. At the given incident energy of 36 meV only the $J:0\rightarrow1$ and $0\rightarrow2$ rotational transitions are allowed as the incident beam comprises only $J=0$ molecules, and the $J=3$ rotational state has an associated rotational energy ~66 meV (well in excess of 36 meV). The peak assignments are, in part, confirmed by the energy resolved angular diffraction

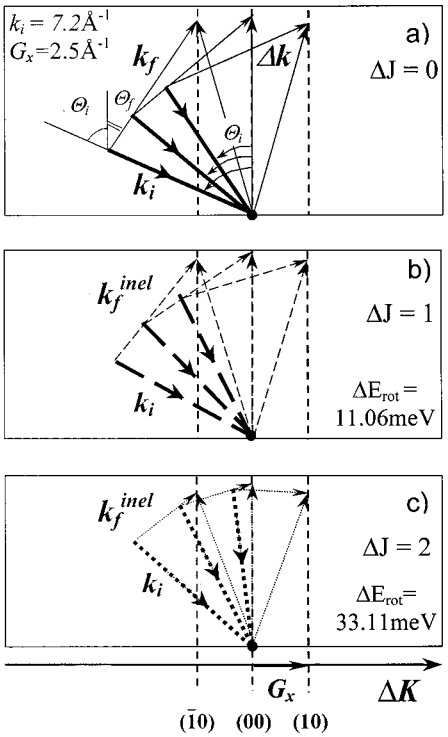

FIG. 4. Ewald representations of the instrumental geometries for HD scattering along the $[1\bar{1}0]$ direction and for incident beam energies of 36 meV. Three different cases are presented separately; (a) no rotational excitation, (b) $J{:}0\rightarrow1$, and (c) $J{:}0\rightarrow2$ rotational excitation. Vertical lines designate the position of reciprocal lattice rods for Cu(001) in the $[1\bar{1}0]$ direction. Note: for inelastic scattering $|\mathbf{k}_f|\neq|\mathbf{k}_i|$. Case (c) shows a kinematic construction for a diffraction intensity peak that is not physically observable. The (10) diffraction condition illustrated in (c) has nonphysical $\mathbf{k}_f$ that does not emerge from the surface ($k_f^Z<0$).

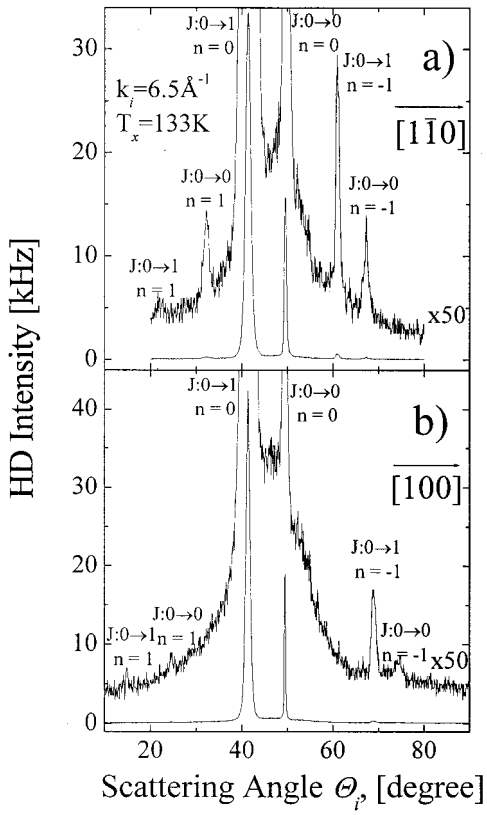

FIG. 5. Angular distributions for HD scattering from the Cu(001) surface at $T_x=133$ K, and $E_i=29$ meV, $k_i=6.5$ Å^{-1}. (a) Total intensity scan taken along the $[1\bar{1}0]$ direction. (b) Total intensity scan taken along the [100] direction.

scans in Figs. 3(b) and 3(c). Figure 3(b) displays the contribution of the total intensity that is truly elastic. In contrast Fig. 3(c) displays an intensity contribution that is associated with an 11.0 ± 0.1 meV translational kinetic energy loss, i.e., a $J{:}0\rightarrow1$ transition on surface scattering. The peak corresponding to the $J{:}0\rightarrow1$ rotational transition and no diffraction (with $n=0$ at $\Theta_i=41.5°$) is the most intense and, especially, this peak is more intense than the true specular peak (with $n=0$ at $\Theta_i=49.5°$) and $\Delta J=0$.

An Ewald representation of the scattering kinematics (Fig. 4), a useful visualization of the scattering processes, is shown in Fig. 4. Figure 4(a) illustrates the case when no rotational excitation occurs. Figures 4(b) and 4(c) show the scattering kinematics for (b) $J{:}0\rightarrow1$ and (c) $J{:}0\rightarrow2$ rotational excitations. The angle between the incoming and outgoing scattering wave vectors is kept constant as the total scattering angle $\Theta_{\text{total}}=\Theta_i+\Theta_f(=99°)$. The incoming ($\mathbf{k}_i$) and outgoing ($\mathbf{k}_f$) wave vectors and the wave vector transfer ($\Delta\mathbf{k}$) rotated about the (000) point as the sample is rotated. The scattering angle for each diffraction condition (Θ_i) is equivalent to the angle between the incident vector $\mathbf{k}_i$ and the surface normal [$\Delta\mathbf{K}=(00)$ line]. The Ewald constructions clearly illustrate that the HD molecules which undergo pure rotational excitations always show corresponding nth order diffraction peaks at smaller scattering angles, Θ_i.

Comparable diffraction features are to be seen in other total angular scans. Figure 5 illustrates two scans taken at a lower HD incident energy ($E_i=29$ meV). The two $n=0$ features remain the most intense. Note, the relative strengths of these two intense features are scarcely affected by the change of the scattering azimuth [compare Figs. 5(a) and 5(b)]. The azimuth does, as anticipated, affect the position and intensities of the $n\neq0$ diffraction peaks.

The temperature dependence of the two intense $n=0$ diffraction peaks have been investigated in Fig. 6. The peak intensity attenuations, with increasing temperature, are consistent with the Debye–Waller (DW) behavior

$$I=I_o e^{-2W}, \tag{1}$$

where W is proportional to the surface temperature. For the rotationally elastic $n=0$ peak it has been suggested[19] that the DW factor is given by

$$2W=\frac{24m(E_i^Z+D)T_x}{Mk_B\Theta_D^2}, \tag{2}$$

where m is the mass of the incident particle, and M is the mass of the surface species. E_i^Z is given by $E_i^Z=E_i\cos^2\Theta_i$ and D is a potential well depth. The data (not shown) indicate a surface Debye temperature, $\Theta_{\text{D(He)}}$, (as seen by the helium atoms) to be approximately 302 K. A value of 269 K in agreement with other workers[16] is achieved only if the well depth is assumed to be ~ 0. For HD scattering the measured Debye temperatures are much lower if the well

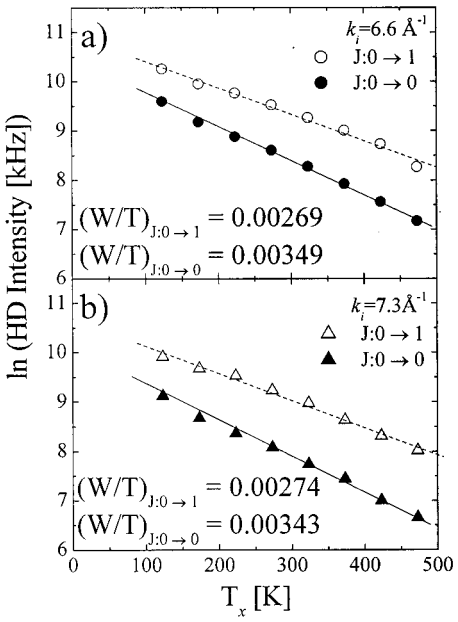

FIG. 6. Temperature variation of the $n=0$ HD diffraction peaks. (a) $E_i=30$ meV, $k_i=6.6$ Å^{-1}; (b) $E_i=37$ meV, $k_i=7.3$ Å^{-1}. Solid symbols represent peak intensities for the elastic (J:0→0) specular reflected peak. Open symbols show the higher rotationally inelastic (J:0→1) $n=0$ diffraction peak intensities. Best fit straight line gradients are displayed for the four curves.

depth is ignored (see tabulated data in Table III). Yet the hydrogen/Cu(001) well depth is well characterized for both H_2 and D_2,[20] and also for HD.[21] Inclusion of the well depth $D_{HD}=30.5$ meV restores $\Theta_{D(HD)}$ to the order of 290 K; this value is also observed for two incident beam energies.[22]

For the rotationally inelastic peaks, the incident k_i^Z is not equivalent to the final k_f^Z. Thus in analysis of the $n=0$ rotationally inelastic peak we have utilized the more general form of Eq. (2);

$$2W=\frac{3\hbar^2(\Delta k_{\mathrm{eff}}^Z)^2T_x}{Mk_B\Theta_D^2}. \tag{3}$$

Equation (3) can also include the Beeby effect[23] of a potential well before a hard wall surface; the effective Δk^Z is raised appropriately. For the rotationally inelastic peak a slightly higher $\Theta_{D(HD)}$ is found (~324 K).

Figures 3 and 5 show not only the coherent diffraction intensity peaks (with $\Delta J=0$, 1 and 2), but also weaker intensity shoulders around both the $n=0$, $\Delta J=0$ and 1 diffraction conditions. The background levels in the scans of Figs. 3(b) and 3(c) suggest that some of the shoulder intensity is incoherent scattering of either the elastic or the purely rotationally inelastic types.

TABLE III. Debye–Waller temperatures.

Scattering species	Incident energy [meV]	Assumed well depth [meV]	Θ_D [K] R.E.	Θ_D [K] R.I.
He	39.0	0	269±4	—
		5.7[a]	302±4	—
HD	29.6	0	155±3	161±4
		30.5[b]	287±7	321±7
	36.6	0	175±3	178±4
		30.5[b]	299±8	327±7

[a]Reference 22.
[b]Reference 21.

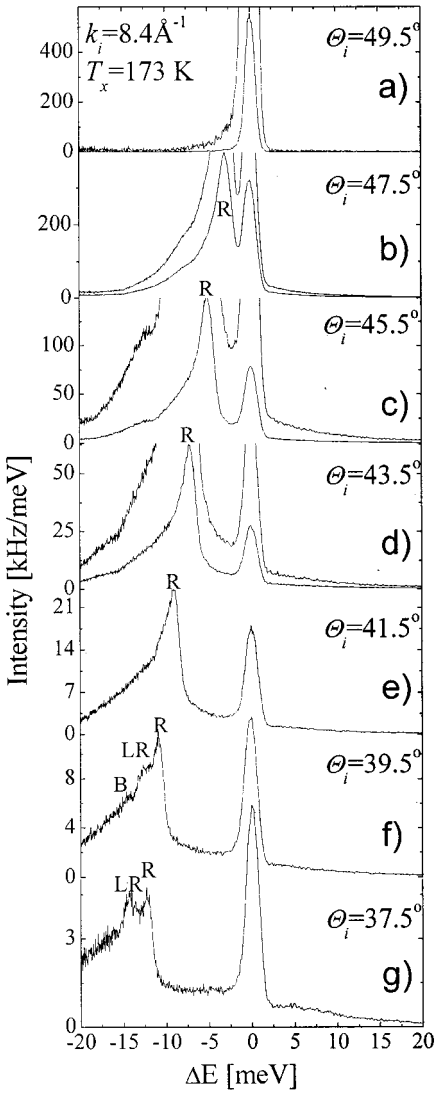

FIG. 7. A series of TOF spectra, converted to the energy transfer scale, for He scattering from Cu(001) along the $[1\bar{1}0]$ direction. All spectra show sharp inelastic peaks which can be attributed to the creation of the vertically polarized surface Rayleigh phonon mode (R). The surface longitudinal resonance (LR) and bulk edge (B) modes can also be observed at incident angles far from the specular ($\Theta_i=49.5°$).

Other inelastic components, namely inelastic phonon scattering, are also present. By a comparison of the time-of-flight spectra for Cu(001) along the $[1\bar{1}0]$ azimuth, measured both with He (Fig. 7) and with HD (Fig. 8), the HD spectra have the additional nondispersing feature at −11.1 meV. Also, while the helium time-of-flight spectra show sharp features which disperse away from the ($\Delta K=0$, $\Delta E=0$) specular condition, the HD spectra have additional inelastic features dispersing from the rotationally inelastic origin ($\Delta K=0$, $\Delta E=-11$ meV).

The helium energy and parallel momentum transfers are

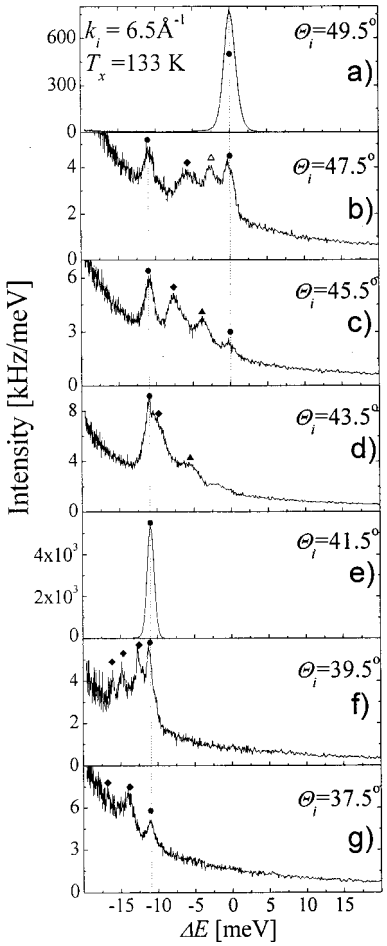

FIG. 8. Typical energy-transformed TOF spectra for HD scattering from the clean Cu(001) surface along the $[1\bar{1}0]$ direction. The rotationally inelastic dispersionless mode $[\Delta E=-\Delta E_{\mathrm{rot}}(0\rightarrow 1)=-11\ \mathrm{meV}]$ is clearly present at all scattering angles. The rotationally elastic peak ($\Delta E=0$ meV) is observed only at angles close to the specular. In the region $\Theta_i=41.5°\rightarrow 49.5°$ two other types of inelastic feature can be identified. One type disperses into the elastic origin, the other to an inelastic origin ($\Delta K=0$, $\Delta E=-\Delta E_{\mathrm{rot}}=-11$ meV). Note that at $\Theta_i<41.5°$ all of the inelastic peaks are of the latter inelastic origin type.

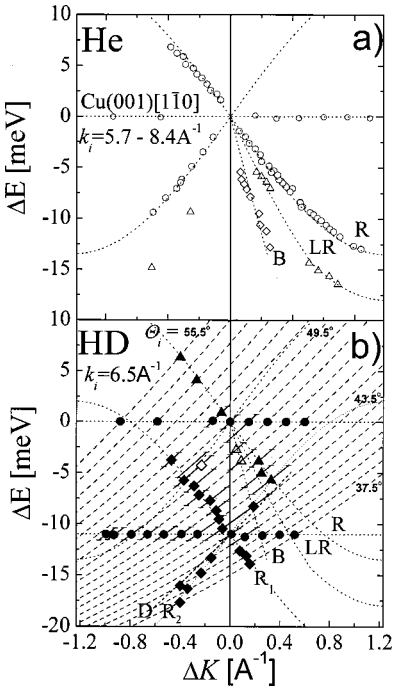

FIG. 9. (a) Dispersion curves of surface and bulk phonon features of the Cu(001) surface measured along the $[1\bar{1}0]$ direction, as measured with He scattering. Data were collected from TOF spectra with incident energies ranging from 17 to 37 meV ($k_i=5.7-8.4$ Å^{-1}); (b) dispersion curves measured with HD beam at $E_i=29$ meV ($k_i=6.5$ Å^{-1}). The position of the Rayleigh wave, longitudinal resonance and bulk edge modes [as measured previously in (a) above with He] are indicated by the dotted lines. The anticipated dispersion associated with Rayleigh phonon modes coupled with rotational excitation are labeled R_1 and R_2. The additional horizontal line at $\Delta E=-\Delta E_{\mathrm{rot}}(0\rightarrow 1)$ shows the dispersionless energy losses expected for pure rotational excitation alone. The near parallel scan curves (running generally from lower left to top right) show the kinematic conditions of the measurements presented in Fig. 8 and provide the wave vector assignments, ΔK, of observed features. Possible positions of decepton features are marked by the short dashed line labeled "*D*."

shown in Fig. 9(a). Several inelastic energy modes are clearly identified: the perpendicular polarized Rayleigh modes (R), the longitudinal resonance modes (LR), and the transverse bulk edge modes (B). The dispersion curves measured here are in good agreement with experimental data obtained by other workers.[16,17] A similar dispersion plot is shown of the HD inelastic modes from Cu(001) along the $[1\bar{1}0]$ direction [Fig. 9(b)]. The bars through data points indicate the full-width-at-half-maximum of the observed features. Bars without data points are drawn to indicate broad plateau regions of intensity. On the same picture, the positions of the helium inelastic scattering modes, i.e., Rayleigh wave (R), longitudinal resonance (LR), and transverse bulk edge (B) [just as in Fig. 9(a)] are indicated by dotted lines, originating from the $\Delta K=0$, $\Delta E=0$ point. For clarity also the Raleigh wave modes, R_1 and R_2 are shown dispersing through the $\Delta K=0$, $\Delta E=-11$ meV origin.

The positions of the so-called "deceptons" have also been mapped out in Fig. 9(b) as a short-dashed line, marked "*D*." Points can arise on this decepton dispersion curve by the false analysis of weak features originating with nonmonochromatic incident particles. They can be observed as distinct features either close to diffraction conditions ($n\neq 0$)[19,24] or, in the case of HD scattering, close to rotational excitations (and diffraction). Observed decepton features near the $\Delta E=-\Delta E_{\mathrm{rot}}(0\rightarrow 1)$ condition are not displayed in this dispersion plot.

Inelastic peaks displayed in the positive energy transfer region can be associated with Raleigh wave modes, similar to those observed in the helium spectra. At $\Delta E<-11.06$ meV all the displayed inelastic peaks can be fitted well to the Raleigh mode curve passing through the $\Delta K=0$, $\Delta E=-11.06$ meV origin. The intermediate ($-11.06<\Delta E<0$ meV) region shows evidence of the two types of modes, i.e., those dispersing from the $\Delta E=0$ origin and those from the $\Delta E=-11$ meV origin. The detailed observations in this region, however, show that simple mode assignment is more complex. Figures 10(a)–10(d) are designed to illustrate the apparent difference of modes seen in helium, and HD scattering. One pair, (a) and (b), shows nearly identically positioned inelastic features for He and HD scattering but, as one concentrates on a region closer to the $\Delta E=0$

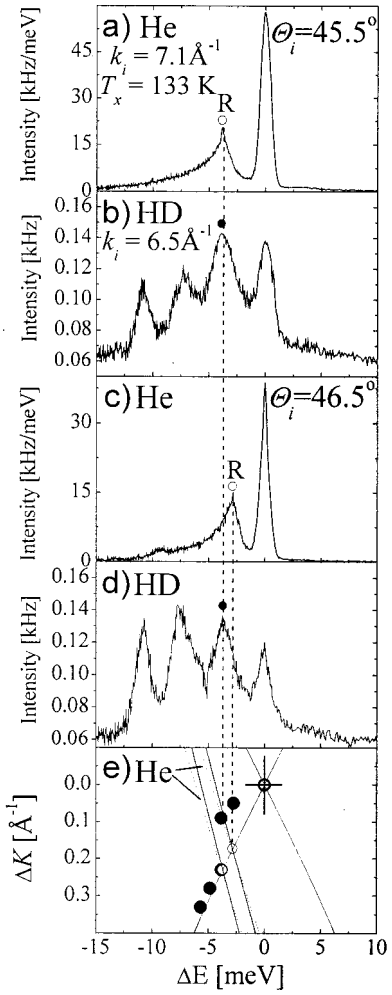

FIG. 10. A comparison of energy-transformed TOF spectra measured with He (a, c) and HD (b, d) at two incident angles ($\Theta_i = 45.5°$ for a–b, 46.5° for c–d). For a clearer comparison the Jacobean transformation was not applied to the HD data. A blow up of the dispersion curves near $\Delta E = 0$, $\Delta K = 0$ region is presented in (e) with He data (open circles) and HD data (closed circles) superimposed. The scan curves for the He scattering are depicted by dotted lines, and those for the HD scattering by solid lines. Incident energies in these He/HD comparison measurements are chosen such that the scan curves run nearly parallel and cross in the $\Delta E = 0$, $\Delta K = 0$ region.

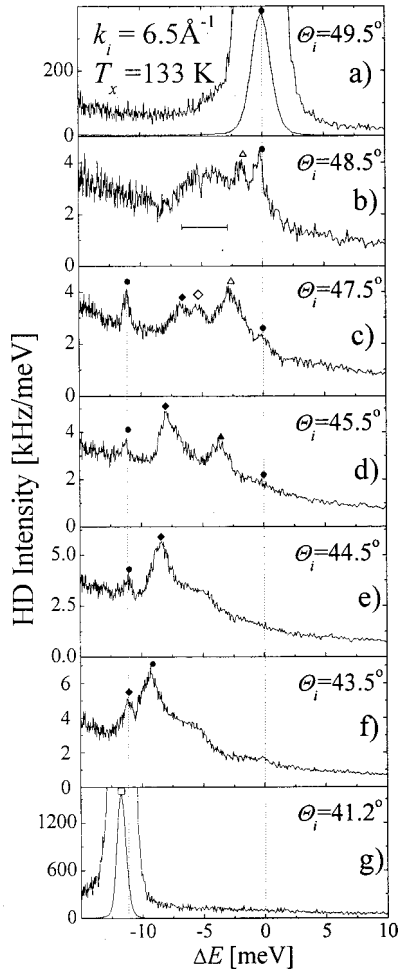

FIG. 11. Energy-transformed TOF spectra for HD scattering from the clean Cu(001) surface along the [100] direction. Note: one TOF scan is shown for $\Theta_i = 41.2°$ (slightly away from the rotationally inelastic peak position). The strong inelastic feature maps onto the deception dispersion curve in Fig. 12.

origin, the other pair of energy-transferred TOF scans, (c) and (d), shows distinctly different intensity peak positions. The apparent mode energy is displaced by as much as 0.8 meV. The simple assignment of the HD inelastic features to the Raleigh wave mode is not possible. Figure 8(c) shows an enlargement of the measured dispersion curves, near the $\Delta K = 0$, $\Delta E = 0$ origin.

Last, a series of TOF measurements, shown in Fig. 11, were performed for HD scattering along the [100] azimuth. These measurements were taken with an identical surface temperature (133 K) and beam energy ($E_i = 29$ meV, $k_i = 6.5$ Å^{-1}) to those used in the measurements shown in Figs. 8 and 9. Figure 12 shows the mapped out dispersion curves along the [100] azimuth. Again, the simple assignment of the HD inelastic features to the Raleigh wave modes is not possible.

IV. DISCUSSION

The main observations are as follows: (i) the most intense HD diffraction peak corresponds to the $J:0 \rightarrow 1$ rotational state transition and zero parallel momentum transfer; (ii) the ratios of the rotationally inelastic $J:0 \rightarrow 1$ $n = 0$ to rotationally elastic $J:0 \rightarrow 0$ $n = 0$ peak intensities (RI/RE) are essentially independent of the scattering azimuth; (iii) the two major elastic and inelastic HD peak intensities show well-behaved Debye–Waller dependence; (iv) the first order diffraction peaks of the rotationally inelastically scattered HD are of significant intensity but are not symmetric; (v) the measured HD phonon dispersion curves do not lie exactly on the surface Raleigh mode dispersion curves.

(i) The molecular charge density contours and the interaction potential of hydrogen with any other molecule cluster or surface are, to first approximation, spherical. Hence, for H_2 and D_2 surface scattering, only a small fraction of the symmetric scattering molecules undergo rotational excitation/de-excitation.[8,20] In contrast, this and other work[13] show that HD has a high probability for rotational excitation on surface scattering. This can be broadly understood within a classical discussion of angular momentum exchanges. For

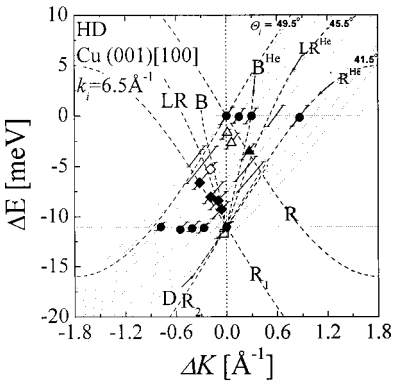

FIG. 12. Dispersion curves of features measured with HD (E_i=29 meV, k_i=6.5 Å^{-1}) from the Cu(001) surface along the [100] direction. For other details, compare directly with Fig. 9(b). Note also, one decepton feature (□) is shown here.

HD the center of mass of the molecule is displaced by a distance $a=0.164$ Å from the molecular electronic center. For a sudden impact, any molecule undergoing a momentum transfer $\hbar\Delta\mathbf{k}$ would also have an angular momentum, $\Delta\mathbf{L}$, imparted to it on scattering:

$$|\Delta\mathbf{L}| \cong a\hbar|\Delta\mathbf{k}|\sin\alpha, \tag{4}$$

where α is the orientation of the molecular axis with respect to the momentum transfer ($\hbar\Delta\mathbf{k}$). For a typical momentum exchange (say $\sim 2\hbar\, k_i^Z$, of order $11\hbar J\,\mathrm{s\,Å}^{-1}$) the imparted angular momentum may be as large as $1.8\hbar$ J s (depending on the instantaneous molecular orientation). Thus it is of no surprise that HD can undergo the 0 to 1 $\hbar$ rotational excitation with high probability on most surfaces, just as is illustrated in Figs. 3 and 5.

(ii) In the above arguments, no reference is made to the nature of the scattering surface. The surface is presumed only to have high specular $n=0$ reflectivity (with little corrugation), and to have a low probability of energy transfer either from, or into, the surface. The above assumptions may be good for Cu: consistently the scattering azimuth apparently does not affect the relative probability of $J:0\rightarrow 1$ and $J:0\rightarrow 0$ processes for $n=0$, i.e., *RI/RE*.

(iii) The simple kinematic argument [assuming $W \propto\langle(\Delta k_{\mathrm{eff}}^Z u_Z)^2\rangle$] explains well the relative magnitudes of the HD Debye–Waller factors of the two $\Delta K=0$ (or $n=0$) HD diffraction peaks. Also, we note that an experimentally determined value for the HD well depth ($D_{\mathrm{HD}}=30.5$ meV) gives consistent values for the surface Debye temperatures, Θ_D, for both HD and He scattering. Unfortunately we could not determine whether the same Debye–Waller behavior extends to H_2 and D_2 scattering on Cu(001). A discrepancy for the homonuclear molecular isotopes was observed for hydrogen scattering from Ag (111).[9]

(iv) The surface corrugation and transfer of perpendicular to parallel energy cannot be ignored for scattering from this surface as the diffraction peaks do represent a significant fraction of the scattered intensity. While Cu(001) exhibits anomalously low first order diffraction peak intensities for helium (a corrugation amplitude below 0.005 Å[19]), HD diffraction features are much more clearly observable in the HD angular scans. Using a simple Eikonal calculation and considering only the intensity in rotationally elastic channels, the "elastic" HD corrugation amplitude is of order 0.06 Å.[24] This corrugation change from He to HD has been explained[25] in terms of a deeper HD physisorption potential well, and the closer approach of HD molecules to the surface than for He atoms with comparable incident energies.

An unorthodox "inelastic" Eikonal approximation could also be applied for the calculation of inelastic diffraction intensities. However, there remains a fundamental problem in the application of any kinematic approach to the inelastic data. Namely, the first order diffraction peaks of the rotationally inelastic HD are not symmetric. For $E_i^{\mathrm{HD}}=36$ meV and $J:0\rightarrow 1$, the $(\bar{1}0)$ peak is approximately five times more intense than for the (10) peak. The asymmetry factor raises to $\sim\times 8$ as E_i is decreased to 29 meV. For a surface with inversion symmetry the asymmetry factor is not expected kinematically, as the perpendicular momentum transfers Δk^Z are identical for both the $J:0\rightarrow 1$ $n=1$ and $n=-1$ peaks. More complete close coupling calculations (beyond the scope of this paper) would be required to accurately reproduce the experimental diffraction intensities. Note also the $n=+1$ diffraction peak for a $J:0\rightarrow 2$ event, is illustrated in Fig. 4(c). This diffraction condition is not physically obtainable, as the "required k_f vector" is directed into the surface. This is an extreme example where clearly, contrary to kinematic calculational approaches, the $n=1$ and $n=-1$ diffraction peaks *cannot* show symmetric intensities. A similar asymmetry was observed for HD A1(001) scattering,[26] also for D_2 NaF scattering.[12] Surprisingly, the asymmetry was not detected (or was not so pronounced) for Ni(001)[13] and for Ag(111).[9,15] In the latter case the instrumental angular resolution was only just sufficient to resolve diffraction peaks. We speculate only that the removal of an asymmetry in the Ni data may be an incidental side effect of other factors pertinent to Ni that we discuss at the end of this section.

(v) The results of the time-of-flight measurements indicate that there is a strong coupling of the HD molecules to surface phonons at the Cu(001) surface. However, it is also apparent, that the strongest coupling is not necessarily to the surface Raleigh modes, such as is the case for He scattering. A similar conclusion was drawn by Berndt *et al.* when considering the HD scattering from the Ni(001) surface. For Ni the dispersion of the measured rotationally inelastic points followed most closely the surface projected bulk band edge over a range from $-0.35\,\mathrm{Å}^{-1}<\Delta K<0.4\,\mathrm{Å}^{-1}$. For Ni(001) [100] the ratio of the transverse bulk edge and Raleigh dispersion gradients is only 1.28 (indicating the excellent accuracy and resolution of the data set[13]). For the Cu(001) $[1\bar{1}0]$ azimuth the gradient ratio of the bulk edge and Raleigh dispersion curves is as high as 2.84. Despite careful measurements, however, we have not been able to assign one edge (or one mode) to the dispersion of the HD/Cu data. The measured dispersion appears to waiver between the Raleigh and the bulk edge. For Cu (001) there is also the possibility of coupling into the longitudinal mode. As a reminder, the longitudinal mode on Cu(001) has an unusually large cross section for the He probe.[16] Can the same be true for HD?

For both scattering azimuths investigated, the widths of

the observed inelastic features, as indicated by bars on the HD diagrams of Figs. 9 and 12, are substantially broader than the instrumental resolution and are often broad enough to include all three (Raleigh, longitudinal, bulk edge) features. Thus HD must couple more strongly than He to either the longitudinal and/or the bulk phonons. We propose therefore that the central peak position is governed by the relative cross sections for the three modes for the two directions. Coupling of HD to the three modes will be tied closely to the azimuth, to impact energies, to energy losses as well as to the exact nature of the surface interaction potential. Enhancement of HD-bulk phonon cross sections (over He-bulk phonon cross sections) may be anticipated as the increased potential well depth of HD allows for closer approach distances and overall stronger coupling.

Last, we wish to make other comparisons with the published data[13] for the Ni(001) surface. A most surprising distinction is that the Cu $J{:}0\rightarrow 1/J{:}0\rightarrow 0$, i.e., "$RI/RE$," ratios (e.g., $RI/RE_{\mathrm{Cu}}\sim 5{:}1$ for $T_x=323\,\mathrm{K}$, $E_i=36\,\mathrm{meV}$; or $\sim 2{:}1$ for $T_x=133\,\mathrm{K}$, $E_i=30\,\mathrm{meV}$) are markedly different from that shown for the Ni surface (e.g., $RI/RE_{\mathrm{Ni}}\sim 20{:}1$ for $T_x=390\,\mathrm{K}$, $E_i=32\,\mathrm{meV}$). Explanation of this distinction could depend on several factors including (a) HD scattering geometries, i.e., Θ_{total}, (b) incident HD beam properties, (c) Debye–Waller factors and surface temperatures, (d) surface defect densities, (e) coincidence with the resonance features, and/or (f) the surface purity, especially adsorped H.

The nickel experiments were performed with an apparatus utilizing $\Theta_{\mathrm{total}}=90°$ compared to ours at 99°. At any given E_i, the magnitude of the elastic momentum transfer vectors, $|\hbar\Delta\mathbf{k}|$, are 8% higher for the Ni experiments than for Cu. The ratio RI/RE is only weakly Δk^Z dependent; factor (a) would raise the peak intensity ratio RI/RE for Ni by only a small fraction (less than 20%). The experimentally observed peak widths, one of which can show velocity spread broadening, are not significantly different from Cu to Ni, as similar HD beam energies and comparable energies resolutions ($\sim$1.5%–2%) were used in both experiments. This implies that factor (b) is insufficient to explain the Cu and Ni RI/RE ratio difference. The bulk Debye temperatures[27] for Cu and Ni are, respectively, 343 K and 450 K. This difference, if mirrored in surface Debye temperatures, would only lead to enhanced RI/RE for Cu compared to Ni; in contrast with the observed distinction. Factor (c) is discounted; it is not contributing to a larger RI/RE for Ni than for Cu. The Ni work showed evidence of coupling of defects with incoherent rotationally inelastic scattering (that is not apparent in this Cu work). But there was no evidence that scattering into incoherent channels preferentially attenuates the coherent *RI* peak intensity over the coherent *RE* peak intensity. Thus factor (d) is disregarded. Regarding (e), in our measurements resonance conditions have been avoided. If the incident energy used in the Ni experiment would have coincided with a resonance condition, then the *RE* intensity would be enhanced (coupling into a resonance maximum) and the *RI* intensity would be reduced (coupling into a resonance minimum[28]). Therefore, an incident energy region coincident with an HD on Ni bond state resonance condition can only reduce the RI/RE ratio. Factor (f) above (namely hydrogen adsorption) is to be prevalent on Ni at the low surface temperature ($T_x=133\,\mathrm{K}$). It is, however, with the adsorbed H species that the RI/RE_{NiH} ratio is restored to a value (e.g., $RI/RE_{\mathrm{NiH}}\sim 6{:}1$ for $T_x=150\,\mathrm{K}$, $E_i=32\,\mathrm{meV}$) that is, comparable with the data seen on other surfaces. An anticipated effect of H adsorption would be the mass induced changing of the vibrationally elastic intensities. A corresponding increase in the Debye–Waller factors with H adsorption would be observed. Thus the anticipated RI/RE ratio ought to increase further with H adsorption, which is contrary to that seen experimentally. We conclude that there is an anomalous RI/RE ratio for the clean Ni surface. Hydrogen adsorption apparently removed this anomalous behavior.

The availability of the HD adsorption channel on Ni is the only, as yet not discounted, factor unique to the clean Ni surface. According to six-dimensional quantum dynamic calculations of dissociative adsorption,[29] H_2 in the $J=0$ state exhibits an enhanced sticking probability on Pd(001) over the other rotationally excited states. The implication for Ni(001) might be that the near surface $J=0$ molecules have a higher probability of accessing a predissociation channel. This channel then either allows complete dissociation or allows further $J{:}0\rightarrow 1$ conversion before coherent reemergence from the surface. Either case would explain a preferred reflection of the rotationally excited HD molecules from the clean Ni surface, i.e., at surface temperatures above that for H_2, HD, or D_2 desorption.

V. SUMMARY

We have measured the angular intensity distributions and time-of-flight spectra for HD scattering from the Cu (001) surface. Both the Cu and Ni(001) surfaces behave similarly in that scattering HD molecules do not couple exclusively to the surface Raleigh phonons: strong HD coupling with bulk phonon modes of the metal surfaces are implied. Coupling of HD to the surface longitudinal modes of copper also cannot be discounted. In addition, we have suggested that Ni(001) showed an unusually low elastic specular feature and have proposed that there is an enhanced probability for the HD in the $J=0$ rotational state to couple into a predissociation channel above the Ni surface.

ACKNOWLEDGMENT

This work was supported by NSF-CHE 9820061.

APPENDIX

The study of inelastic scattering processes, using atomic and molecular beams, ideally requires back-scattered energy determinations to a precision of order $\pm$ 0.1 meV or better. This degree of precision demands very accurate measurements of both times-of-flight as well as the time-of-flight distances. Typically, flight distances cannot be measured so accurately within UHV chambers. Also, the ionization region of the detector is elongated and it is not possible to predict the position of maximum ionization probability. Thus one approach to calibration of the distances is to use a standard such as the rotational energy gain and transnational energy

loss for HD undergoing a $J=0$ to $J=1$ transition ($\Delta E_{\mathrm{rot}} = 11.063\,\mathrm{meV}$). The analysis used here for the time-of-flight distances and the total scattering angle determination involved a number of details that are described below.

Time-of-flight distances

For a rotational transition, the conservation of energy gives:

$$E_i = E_f - \Delta E_{\mathrm{rot}}, \tag{A1}$$

where ΔE_{rot} is the change in transnational energy of a rotationally excited molecule, far from the surface. The rotational energy is considered to have a precise (gas-phase) quantum value (-11.063 meV) for the $J{:}0\rightarrow 1$ excitation. The energy terms can be expressed in terms of the velocity of the particles in the following manner:

$$E_i = \frac{m v_i^2}{2} = \frac{m}{2}\left(\frac{S_{\mathrm{CD}}}{t_{\mathrm{CD,elast}}}\right)^2 \tag{A2}$$

and

$$E_f = \frac{m v_f^2}{2} = \frac{m}{2}\left(\frac{S_{\mathrm{TD}}}{t_{\mathrm{TD}}}\right)^2, \tag{A3}$$

where S is distance, t is time-of-flight and indexes C, T, and D stand, respectively, for chopper, target (crystal), and detector. Substitution into Eq. (A1) gives

$$\Delta E_{\mathrm{rot}} = \frac{m}{2}\left\{\left(\frac{S_{\mathrm{TD}}}{t_{\mathrm{CD,inel}} - t_{\mathrm{CD,elast}}\left(1 - \frac{S_{\mathrm{TD}}}{S_{\mathrm{CD}}}\right)}\right)^2 - \left(\frac{S_{\mathrm{CD}}}{t_{\mathrm{CD,elast}}}\right)^2\right\}.$$

The last equation includes $t_{\mathrm{CD,elast}}$ and $t_{\mathrm{CD,inel}}$ which are experimentally observable flight times. The suffix ''inel'' refers to the observed inelastic time of feature that corresponds to the pure $J{:}0\rightarrow 1$ transition. The independent determination of the flight distances S_{TD} and S_{CD} is achieved through a minimum of two data sets (each with a $t_{\mathrm{CD,elast}}$ and $t_{\mathrm{CD,inel}}$ pair) taken with differing incident energy values, E_i. Self-consistency is also checked with additional data sets.

Total scattering angle

The value of the total scattering angle Θ (angle between incoming and outgoing beams: $\Theta_{\mathrm{total}} = \Theta_i + \Theta_f$) has also been calibrated:

$$\Theta_f = \Theta_{\mathrm{total}} - \Theta_i. \tag{A4}$$

The conservations of energy and of parallel momentum components can be stated:

$$\frac{\hbar^2 k_i^2}{2m} = \frac{\hbar^2 k_f^2}{2m} + \Delta E_{\mathrm{rot}}, \tag{A5}$$

$$\mathbf{K}_i = \mathbf{K}_f + \mathbf{G}, \tag{A6}$$

where k_i, k_f are the magnitude of the incident and final molecular wave vectors, m is a molecular mass of HD, $\mathbf{K}$ is the parallel component of the incident wave vector, $\mathbf{G}$ is a surface reciprocal lattice vector, and ΔE_{rot} is the transfer of transnational to rotational energy (if any). The parallel projections of the incoming and outgoing wave vectors Eq. (A6) can be restated in the following way:

$$\begin{aligned} k_i \sin\Theta_i \pm nG_x &= \sqrt{k_i^2 + \frac{2m\Delta E_{\mathrm{rot}}}{\hbar^2}}\sin(\Theta_{\mathrm{total}} - \Theta_i) \\ &= k_f \sin(\Theta_{\mathrm{total}} - \Theta_i), \end{aligned} \tag{A7}$$

where G_x is the projection of the reciprocal vector, $\mathbf{G}$, on the scattering plane. Equation (A7) gives us the unique positions of all the elastic and rotationally inelastic diffraction peaks and an expression for the incident scattering angle in terms of the total scattering angle:

$$\sin\Theta_i(n) = \frac{nG_x\left(\frac{k_i}{k_f} + \cos\Theta_{\mathrm{total}}\right) + \sin\Theta_{\mathrm{total}}\sqrt{k_i^2 + k_f^2 + 2k_i k_f \cos\Theta_{\mathrm{total}} - n^2 G_x^2}}{\frac{k_i^2}{k_f} + 2k_i\cos\Theta_{\mathrm{total}} + k_f}. \tag{A8}$$

Only the relative positions for various $\Theta_i(n)$ are easily measured, as initially there is an unknown offset in Θ_i. In practice, the offset together with the one value for Θ_{total} are established by checking for self-consistency for many diffraction conditions; typically at $n=0$, for large n, and for varying E_i.

[1] H. A. Michelsen, C. T. Rettner, and D. J. Auerbach, Phys. Rev. Lett. **69**, 2678 (1992).
[2] C. T. Rettner, D. J. Auerbach, and H. A. Michelsen, Phys. Rev. Lett. **68**, 2547 (1992).
[3] G. D. Kubiak, G. O. Sitz, and R. N. Zare, J. Chem. Phys. **83**, 2538 (1985).
[4] C. T. Rettner, H. A. Michelsen, and D. J. Auerbach, J. Vac. Sci. Technol. B **11**, 1901 (1993).
[5] C. T. Rettner and D. J. Auerbach, J. Chem. Phys. **104**, 2732 (1996).
[6] C. T. Rettner and D. J. Auerbach, Phys. Rev. Lett. **74**, 4551 (1995).
[7] U. Harten, J. P. Toennies, and Ch. Wöll, J. Chem. Phys. **85**, 2249 (1986).
[8] S. Andersson and M. Persson, Phys. Rev. Lett. **70**, 202 (1993).
[9] Ch. Yu, K. B. Whaley, C. S. Hogg, and S. J. Sibener, J. Chem. Phys. **83**, 4217 (1985).
[10] J. P. Cowin, Ch. Yu, and L. Wharton, Surf. Sci. **161**, 221 (1985).
[11] F. Hofmann, J. P. Toennies, and J. P. Manson, J. Chem. Phys. **101**, 10155 (1994).
[12] G. Benedek, J. Ellis, N. S. Luo, A. Reichmuth, P. Ruggerone, and J. P. Toennies, Phys. Rev. B **48**, 4917 (1993).
[13] J. P. Cowin, Ch. Yu, S. J. Sibener, and L. Wharton, J. Chem. Phys. **79**, 3537 (1983).
[14] Ch. Yu, C. S. Hogg, J. P. Cowin, K. B. Whaley, J. C. Light, and S. J. Sibener, Isr. J. Chem. **22**, 305 (1982).
[15] W. Allison and B. Feuerbacher, Phys. Rev. Lett. **45**, 2040 (1980).
[16] G. Brusdeylins and J. P. Toennies, Surf. Sci. **126**, 647 (1983).
[17] R. Berndt, J. P. Toennies, and Ch. Wöll, J. Chem. Phys. **92**, 1468 (1990).

[18] J. E. Pollard, D. J. Trevor, Y. T. Lee, and D. A. Shirley, J. Chem. Phys. **77**, 4818 (1982).
[19] G. Boato, in *Atomic and Molecular Beam Methods*, edited by Giacinto Scoles (Universal Press, Oxford, 1992), Vol. 2, Part II.12, pp. 340–365.
[20] S. Andersson, L. Wilzén, and M. Persson, Phys. Rev. B **38**, 2967 (1988).
[21] L. V. Goncharova, B. J. Hinch, M. Hassel, and M. Persson, Chem. Phys. Lett. (to be published).
[22] A. Chizmeshya and E. Zaremba, Surf. Sci. **268**, 432 (1992).
[23] J. L. Beeby, J. Phys. C **4**, L359 (1971).
[24] R. B. Doak, in *Atomic and Molecular Beam Methods*, edited by Giacinto Scoles (Universal Press, Oxford, 1992), Vol. 2, Part II.14, pp. 384–443.
[25] In using these simple Eikonal approximations, any resonance features associated with rotationally mediated selective adsorption are ignored. Suffice to say that at the incident energies of the studies used here, HD selective adsorption features can give rise to diffraction intensity variations as large as 30%. Thus the corrugation amplitudes derived from these measurements can be considered only as very rough estimates.
[26] M. Gester, Diploma thesis, Göttingen University, 1987.
[27] Ch. Kittel, *Introduction to Solid State Physics*, 7th ed. (Wiley, New York, 1996), p. 126.
[28] R. Schinke, Surf. Sci. **127**, 283 (1983).
[29] A. Gross, S. Wilke, and M. Scheffler, Phys. Rev. Lett. **75**, 2718 (1995).